PERGAMON

International Journal of Engineering Science 38 (2000) 1993–2011

International Journal of Engineering Science

www.elsevier.com/locate/ijengsci

Magnetoelectroelastic multi-inclusion and inhomogeneity problems and their applications in composite materials

Jiang Yu Li *

Division of Engineering and Applied Science, California Institute of Technology, Mail Code 104-44, Pasadena, CA 91125, USA

Received 23 June 1999; received in revised form 15 November 1999; accepted 10 December 1999

Abstract

We have studied the average magnetoelectroelastic field in a multi-inclusion or inhomogeneity embedded in an infinite matrix. The magnetoelectroelastic inclusion and inhomogeneity problems are discussed [1], and a numerical algorithm to evaluate the magnetoelectroelastic Eshelby's tensors for the general material symmetry and ellipsoidal inclusion shape is developed. The solutions for the magnetoelectroelastic inclusion and inhomogeneity problems are applied to study the multi-inclusion and inhomogeneity problems. It is shown that the average field in an annulus surrounding an inclusion embedded in an infinite magnetoelectroelastic medium only depends on the shapes and orientations of two ellipsoids, which generalizes Tanaka and Mori's observation in elasticity [2]. The average field in a multi-inclusion is then determined exactly, from which the average field in a multi-inhomogeneity is obtained, using the equivalent-inclusion concept [3]. The solutions of multi-inclusion and inhomogeneity problems serve as basis for an averaging scheme to model the effective magnetoelectroelastic moduli of heterogeneous materials, which generalizes Nemat-Nasser and Hori's multi-inclusion model in elasticity [4]. The model is further extended to predict the effective thermal moduli of the heterogeneous magnetoelectroelastic solids, generalizing the recent work of Li on the thermal expansion coefficients of elastic composites [5]. The proposed model recovers Mori–Tanaka and self-consistent approaches as special cases. Finally, some numerical results are given to demonstrate the applicability of the model. The potential techniques to enhance the magnetoelectric effect in practical composites are also discussed.

1. Introduction

Composite material consisting of a piezoelectric phase and a piezomagnetic phase has drawn significant interest in recent years, due to the rapid development in adaptive material systems. It

* Tel.: +1-626-395-4178; fax: +1-626-568-2719.
E-mail address: jjli@its.caltech.edu (J.Y. Li).

PII: S0020-7225(00)00014-8

shows a remarkably large magnetoelectric coefficient, the coupling coefficient between static electric and magnetic fields, which does not exist in either constituent. The magnetoelectric coupling in the composite is created through the interaction between the piezoelectric phase and the piezomagnetic phase, a result of the so-called product property. The product property of composites offers great opportunities to engineer new materials that are capable of responding in a desired way to the internal or environment changes, which may not be achieved otherwise by traditional techniques. Thus a micromechanics analysis of magnetoelectroelastic solids, which may be used to study the property–structure relationship of materials, and to guide the design and optimization of the new materials, will be very helpful.

Since Van Run et al. [6] reported the fabrication of $BaTiO_3$–$CoFe_2O_4$ composite with magnetoelectric coefficient two orders larger than that of Cr_2O_3, which had the highest magnetoelectric coefficient among single-phase materials known at that time, numerous researchers have investigated the magnetoelectric coupling in the piezoelectric–piezomagnetic composites both theoretically and experimentally. Bracke and Van Vliet reported [7] a broad band magnetoelectric transducer with a flat frequency response using composite materials. Harshe et al. [8,9] and Avellaneda and Harshe [10] studied the 2–2, 3–0, and 0–3 magnetoelectric composites theoretically on a case-by-case basis. They obtained expressions for the effective magnetoelectric coefficients and a figure of merit for magnetoelectric coupling. Nan [11] and Huang and Kuo [12] proposed micromechanics models to estimate the effective properties of piezoelectric–piezomagnetic composite materials. Benveniste obtained exact connections between different components of the effective magnetoelectroelastic moduli of fibrous composite [13], using the uniform field concept [14]. Li and Dunn developed a micromechanics approach to analyze the average fields and effective moduli of heterogeneous media that exhibit full coupling between stationary elastic, electric, and magnetic fields [15], using the solutions they obtained for inclusion and inhomogeneity problems in an infinite magnetoelectroelastic medium [1]. They obtained the closed-form expressions for the effective moduli of fibrous and laminated composites, as well as the exact connections between the effective thermal moduli and the effective magnetoelectroelastic moduli of two-phase composites.

This work is along lines of Li and Dunn's work on magnetoelectroelastic inclusion and inhomogeneity problems [1], which generalized Eshelby's classical analyses of the stress- and strain-fields in elastic solids containing ellipsoidal inclusions and inhomogeneities [3]. Eshelby's solutions are widely used in micromechanics analysis of heterogeneous materials for at least three reasons: (1) the general ellipsoidal shape can be used to model a wide range of microstructural geometries; (2) explict, closed-form expressions exist for the stresses and strains in the ellipsoidal inhomogeneity; and (3) the elastic fields in the ellipsoidal inhomogeneity are uniform, trivializing the computation of average fields. Numerous examples of and references to such applications can be found in the texts of Mura [16] and Nemat-Nasser and Hori [17]. Based on the uniformity of strain field in an ellipsoidal inclusion with uniform eigenstrain, Tanaka and Mori showed that the average strain field in an annulus (between two similar and coaxial ellipsoidal surfaces) surrounding an inclusion vanishes [2]. From this observation, they proposed a method, which is credited as the Mori–Tanaka approach later, to analyze the average field in a composite material [18]. Tanaka and Mori's theorem was applied by Nemat-Nasser and Hori to determine the average field in a multi-inclusion embedded in an infinite matrix exactly [17], from which they proposed the double- and multi-inclusion models to predict the effective elastic moduli of composite materials [4]. It is shown that the Mori–Tanaka approach and another popular averaging scheme, self-consistent approach, are special cases of the multi-inclusion model. Li extended the multi-inclusion model to analyze the thermal field and the effective thermal moduli of elastic composites [5]. He demonstrated that this model is particularly suitable for the analysis of composites with functionally graded interphase. Motivated by the success of application of inclusion and inhomogeneity problems in heterogeneous elastic materials, this work intends to generalize Tanaka and Mori's theorem and Nemat-Nasser and Hori's multi-inclusion model to analyze the heterogeneous magnetoelectroelastic solids. It is believed that such a study will be helpful to the micromechanics analysis of heterogeneous magnetoelectroelastic materials. The progress in inclusion and inhomogeneity problems in solid with coupled-field behavior is due to Deeg [19], Wang [20], Benveniste [21], Dunn and Taya [22], Chen [23,24], Dunn and Wienecke [25,26], and Li and Dunn [1], among others, who extended Eshelby's analysis to solid with coupling effects.

The paper is organized as follows. The basic equations and notation will be introduced in Section 2. The multi-inclusion and inhomogeneity problems will be analyzed in Section 3, where we will review the solution of magnetoelectroelastic inclusion problem, develop a numerical algorithm to evaluate the magnetoelectroelastic Eshelby's tensors for general material symmetry and ellipsoidal inclusion shape, generalize the Tanaka–Mori theorem, and use it to determine the average field in a multi-inclusion or inhomogeneity embedded in an infinite magnetoelectroelastic medium. We will then generalize the multi-inclusion model to predict the effective magnetoelectroelastic moduli of composites in Section 4, and further extend it to estimate the effective thermal moduli of the heterogeneous materials. Finally, some numerical results will be presented to demonstrate the applicability of the model.

2. Basic equations and notation

We consider magnetoelectroelastic media that exhibit linear, static, anisotropic coupling between the magnetic, electric, and elastic fields. In this case, the constitutive equations can be expressed as:

$$\begin{aligned}\sigma_{ij} &= C_{ijkl}\varepsilon_{kl} + e_{ijl}(-E_l) + q_{ijl}(-H_l) - \lambda_{ij}\theta,\\ D_i &= e_{ikl}\varepsilon_{kl} - \kappa_{il}(-E_l) - a_{il}(-H_l) - p_i\theta,\\ B_i &= q_{ikl}\varepsilon_{kl} - a_{il}(-E_l) - \mu_{il}(-H_l) - m_i\theta.\end{aligned} \tag{1}$$

Here σ_{ij} and ε_{ij} are the elastic stress and strain; D_i and E_i are the electric displacement and field; B_i and H_i are the magnetic flux and field. C_{ijkl}, κ_{il}, and μ_{il} are the elastic stiffness, the dielectric, and magnetic permeability tensors. They directly connect like fields, e.g., stresses to strains. Elastic field is coupled to the electric and magnetic fields through the piezoelectric, e_{ijl}, and piezomagnetic, q_{ijl}, coefficients, respectively, while electric and magnetic fields are coupled through the magnetoelectric coefficient, a_{il}. Finally, the stress, electric displacement, and magnetic flux are coupled to temperature change θ through thermal stress tensor λ_{ij}, pyroelectric coefficient p_i, and pyromagnetic coefficient m_i. The symmetry conditions satisfied by the moduli are give by Nye [27].

In the analysis that follows, it is convenient to treat the elastic, electric, and magnetic fields on equal footing. To this end, the notation introduced by Barnett and Lothe [28] for piezoelectric analysis and generalized to incorporate magnetic coupling by Alshits et al. [29] is utilized. This notation is identical to conventional indicial notation with the exception that lowercase subscripts take on the range $1 \to 3$, while uppercase subscripts take on the range $1 \to 5$ and repeated uppercase subscripts are summed over $1 \to 5$. With this notation, the field variables take the following forms:

$$\Sigma_{iJ} = \begin{cases} \sigma_{ij}, & J = 1,2,3, \\ D_i, & J = 4, \\ B_i, & J = 5, \end{cases} \qquad Z_{Mn} = \begin{cases} \varepsilon_{mn}, & M = 1,2,3, \\ -E_n, & M = 4, \\ -H_n, & M = 5, \end{cases} \tag{2}$$

the magnetoelectroelastic moduli are expressed as:

$$\hat{E}_{iJMn} = \begin{cases} C_{ijmn}, & J,M = 1,2,3, \\ e_{ijn}, & M = 4,\ J = 1,2,3, \\ q_{ijn}, & M = 5,\ J = 1,2,3, \\ e_{imn}, & J = 4,\ M = 1,2,3, \\ -\kappa_{in}, & J = 4,\ M = 4, \\ -a_{in} & J = 4,\ M = 5, \\ q_{imn}, & J = 5,\ M = 1,2,3, \\ -a_{in}, & J = 5,\ M = 4, \\ -\mu_{in}, & J = 5,\ M = 5, \end{cases} \qquad \Pi_{iJ} = \begin{cases} \lambda_{mn}, & J = 1,2,3, \\ p_i, & J = 4, \\ m_i, & J = 5, \end{cases} \tag{3}$$

and the constitutive equations can be written as:

$$\Sigma_{iJ} = \hat{E}_{iJMn} Z_{Mn} - \Pi_{iJ}\theta = \hat{E}_{iJMn}(Z_{Mn} - Z^{\mathrm{T}}_{Mn}), \tag{4}$$

where $Z^{\mathrm{T}}_{Mn} = \hat{E}^{-1}_{MniJ}\Pi_{iJ}\theta$; the superscript -1 is used to denote inversion. Of course, one can easily make alternative choices for the independent and dependent variables and formulate the basic equations using the same formalism. The current representation is proven to be advantageous in solving inclusion and inhomogeneity problems.

For a heterogeneous material subjected to external loading Z^0_{Kl} at the boundary, and a uniform temperature change θ, the effective magnetoelectroelastic moduli $\hat{E}^*_{iJKl}$ and thermal moduli Π^*_{iJ} can be defined under the assumption of statistical homogeneity by

$$\langle \Sigma_{iJ} \rangle = \hat{E}^*_{iJKl}\langle Z_{Kl} \rangle - \Pi^*_{iJ}\theta, \tag{5}$$

where $\langle \cdot \rangle = 1/V \int_V (\cdot)\,\mathrm{d}V$ denotes an average over a representative volume element (RVE). The modeling of the effective moduli of heterogeneous material in terms of its microstructure and constituent properties is of both theoretical and practical importance in micromechanics. It depends on the determination of the average fields in the materials. In this work we will present an approximation scheme to predict the effective magnetoelectroelastic moduli based on the exact average field in a multi-inclusion embedded in an infinite medium.

3. Multi-inclusion and inhomogeneity problems

We will adopt Mura's terminology here [16]. By inclusion, we mean a subdomain Ω in an infinite matrix D with the same magnetoelectroelastic moduli $\hat{E}_{iJKl}$ as that of the matrix, but undergoing an eigenfield Z^{T}_{Kl}, which, for example, can be associated with spontaneous electric polarization, magnetic moment, and deformations that occur during a crystallographic phase transformation. The eigenfield Z^{T}_{Kl} is that which would occur if Ω were unconstrained by D. Actual constrained magnetoelectroelastic field inside the inclusion is in general a function of material moduli of the matrix, the shape and orientation of the inclusion, and the distribution of eigenfield in the inclusion. By inhomogeneity we mean a subdomain Ω in an infinite matrix D with a different magnetoelectroelastic moduli $\hat{E}'_{iJKl}$ from that of the matrix, $\hat{E}_{iJKl}$. It is possible for the inhomogeneity to undergo an eigenfield. In this case, it is referred to as an inhomogeneous inclusion.

3.1. Magnetoelectroelastic inclusion problem

The magnetoelectroelastic inclusion problem will be reviewed here. A numerical algorithm to evaluate the magnetoelectroelastic Eshelby's tensors will also be developed. The field in an infinite medium with magnetoelectroelastic moduli $\hat{E}_{iJAb}$, due to the presence of an inclusion Ω with arbitrary shape and eigenfield $Z^{\mathrm{T}}_{Ab}(\mathbf{x})$, can be expressed as:

$$Z_{Mn}(\mathbf{x}) = -\int_{\Omega} \hat{E}_{iJAb} Z^{\mathrm{T}}_{Ab}(\mathbf{x}') G_{MJ,in}(\mathbf{x}-\mathbf{x}')\,\mathrm{d}V(\mathbf{x}'), \tag{6}$$

where the subscript "," is used to denote partial differentiation, and G_{MJ} are the infinite-body magnetoelectroelastic Green's functions, whose physical interpretation is given in Table 1. Note that the magnetic monopole is a pure mathematical concept, which will simplify the analysis of inclusion problem. When the inclusion Ω is ellipsoidal and the eigenfield Z^{T}_{Ab} is uniform, the magnetoelectroelastic fields in the inclusion is also uniform and given by

$$Z_{Mn} = S_{MnAb} Z^{\mathrm{T}}_{Ab} \tag{7a}$$

Table 1
Physical interpretation of magnetoelectroelastic Green's functions

$G_{MJ}(\mathbf{x}-\mathbf{x}')$	Physical interpretation
$G_{mj}(\mathbf{x}-\mathbf{x}')$	The elastic displacement at $\mathbf{x}$ in the x_m direction due to a unit point force at $\mathbf{x}'$ in the x_j direction
$G_{m4}(\mathbf{x}-\mathbf{x}')$	The elastic displacement at $\mathbf{x}$ in the x_m direction due to a unit point charge at $\mathbf{x}'$
$G_{m5}(\mathbf{x}-\mathbf{x}')$	The elastic displacement at $\mathbf{x}$ in the x_m direction due to a unit point magnetic monopole at $\mathbf{x}'$
$G_{4j}(\mathbf{x}-\mathbf{x}')$	The electric potential at $\mathbf{x}$ due to a unit point force at $\mathbf{x}'$ in the x_j direction
$G_{44}(\mathbf{x}-\mathbf{x}')$	The electric potential at $\mathbf{x}$ due to a unit point charge at $\mathbf{x}'$
$G_{45}(\mathbf{x}-\mathbf{x}')$	The electric potential at $\mathbf{x}$ due to a unit point magnetic monopole at $\mathbf{x}'$
$G_{5j}(\mathbf{x}-\mathbf{x}')$	The magnetic potential at $\mathbf{x}$ due to a unit point force at $\mathbf{x}'$ in the x_j direction
$G_{54}(\mathbf{x}-\mathbf{x}')$	The magnetic potential at $\mathbf{x}$ due to a unit point charge at $\mathbf{x}'$
$G_{55}(\mathbf{x}-\mathbf{x}')$	The magnetic potential at $\mathbf{x}$ due to a unit point magnetic monopole at $\mathbf{x}'$

with

$$S_{MnAb} = -\int_{\Omega} \hat{E}_{iJAb} G_{MJ,in}(\mathbf{x}-\mathbf{x}')\,\mathrm{d}V(\mathbf{x}'), \tag{8}$$

where S_{MnAb} are the magnetoelectroelastic Eshelby's tensors, which are functions of magneto-electroelastic moduli of the matrix and shape and orientation of the inclusion [1,3]. It can be expressed as surface integrals over a unit sphere,

$$S_{MnAb} = \frac{E_{iJAb}}{4\pi} \begin{cases} \frac{1}{2}\int_{-1}^{1}\int_{0}^{2\pi}[J_{mJin}(\mathbf{z}) + J_{nJim}(\mathbf{z}]\,\mathrm{d}\theta\,\mathrm{d}\xi_3, & M = 1,2,3, \\ \int_{-1}^{1}\int_{0}^{2\pi} J_{4Jin}(\mathbf{z})\,\mathrm{d}\theta\,\mathrm{d}\xi_3, & M = 4, \\ \int_{-1}^{1}\int_{0}^{2\pi} J_{5Jin}(\mathbf{z})\,\mathrm{d}\theta\,\mathrm{d}\xi_3, & M = 5, \end{cases} \tag{9a}$$

where $z_i = \xi_i/a_i$ (no summation on i), and ξ_1 and ξ_2 can be expressed in terms of ξ_3 and θ by $\xi_1 = \sqrt{1-\xi_3^2}\cos\theta$ and $\xi_2 = \sqrt{1-\xi_3^2}\sin\theta$. In addition, $J_{MJin} = z_i z_n K_{MJ}^{-1}(\mathbf{z})$, where K_{MR}^{-1} is the inverse of $K_{JR} = z_i z_n \hat{E}_{iJRn}$. The corresponding Σ_{iJ} in inclusion is then given by

$$\Sigma_{iJ} = \hat{E}_{iJMn}(Z_{Mn} - Z_{Mn}^{\mathrm{T}}) = \hat{E}_{iJMn}(S_{MnAb} - I_{MnAb})Z_{Ab}^{\mathrm{T}}, \tag{7b}$$

where I_{MnAb} is composed of second and fourth rank unit tensors. From Eqs. (7a) and (7b), it is clear that the magnetoelectroelastic field in the inclusion is completely determined if the Eshelby's tensors are known. Li and Dunn have obtained the closed-form expressions of magnetoelectro-elastic Eshelby's tensors for the aligned elliptic–cylindrical inclusion and thin-disc inclusion in a transversely isotropic medium [1]. For more general material symmetry and ellipsoidal inclusion shape, the Eshelby's tensor can be evaluated numerically using Gauss quadrature method [30,31], where the integral is approximated by the weighted sum of function values at certain integration points,

$$S_{MnAb} = \frac{\hat{E}_{iJAb}}{4\pi} \begin{cases} \frac{1}{2}\sum_{p=1}^{U}\sum_{q=1}^{V}[J_{mJin}(z^{pq}) + J_{nJim}(\mathbf{z}^{pq})]W^{pq}, & M = 1,2,3, \\ \sum_{p=1}^{U}\sum_{q=1}^{V} J_{4Jin}(\mathbf{z}^{pq})W^{pq}, & M = 4, \\ \sum_{p=1}^{U}\sum_{q=1}^{V} J_{5Jin}(\mathbf{z}^{pq})W^{pq}, & M = 5. \end{cases} \tag{9b}$$

In Eq. (9b), the superscripts p and q are used to denote the integration points (abscissas) ξ_3^p with weight coefficient W_ξ^p, and θ^q with weight coefficient W_θ^q, from which z^{pq} is evaluated; U and V refer to the corresponding total integration points which can be selected according to the inclusion shape aspect ratios a_1/a_3 and a_2/a_3. $W^{pq} = W_\xi^p W_\theta^q$ is the Gaussian weighting coefficient. An algorithm to evaluate magnetoelectroelastic Eshelby's tensors is developed and outlined in Table 2.

Table 2
Numerical procedure for evaluation of magnetoelectroelastic Eshelby's tensors

Step	Operation
1	Input the magnetoelectroelastic moduli $\hat{E}_{iJKl}$ of matrix, shape aspect ratios of a_2/a_1 and a_3/a_1 of inclusion, and pre-determined numbers of abscissas U and V to be used in Gaussian quadrature method
2	Determine ξ_3^p and θ^q, and the corresponding weighting coefficients W^{pq} according to U and V
3	Evaluate $z_1^{pq} = \sqrt{1-(\xi_3^p)^2}\cos\theta^q/a_1$, $z_2^{pq} = \sqrt{1-(\xi_3^p)^2}\sin\theta^q/a_2$ and $z_3^{pq} = \xi_3^p/a_3$
4	Evaluate $K_{JR}^{pq} = z_i^{pq} z_n^{pq} \hat{E}_{iJRn}$ (no summation on p and q), and its inverse $(K_{JR}^{pq})^{-1}$
5	Evaluate $J_{MJin}^{pq} = z_i^{pq} z_n^{pq} (K_{MJ}^{pq})^{-1}$ (no summation on p and q)
6	Evaluate S_{MnAb} according to Eq. (9b)

3.2. Generalized Tanaka–Mori theorem

Let us consider a finite inclusion Ω_0 with arbitrary shape and eigenfield $Z_{Mn}^{\mathrm{T}}(\mathbf{x})$, embedded in an infinite matrix D with magnetoelectroelastic moduli $\hat{E}_{iJAb}$, and surrounded by two fictitious ellipsoidal surfaces Ω_1 and Ω_2 (not necessarily similar and coaxial), where Ω_1 is totally contained within Ω_2; see Fig. 1. When there is no external loading Z_{Mn}^0 applied at the boundary of the infinite matrix, the average magnetoelectroelastic field in the annulus between Ω_2 and Ω_1, according to Eq. (6), is given by

$$\langle Z_{Mn}(\mathbf{x})\rangle = -\frac{1}{V_2}\int_{\Omega_2-\Omega_1}\left[\int_{\Omega_0}\hat{E}_{iJAb}Z_{Ab}^{\mathrm{T}}(\mathbf{x}')G_{MJ,in}(\mathbf{x}-\mathbf{x}')\,\mathrm{d}V(\mathbf{x}')\right]\mathrm{d}V(\mathbf{x}), \tag{10}$$

where V_2 is the volume of the annulus. Since Ω_0 and annulus do not intersect, and the integrand in Eq. (10) is not singular, the order of integration can be changed to yield

$$\langle Z_{Mn}(\mathbf{x})\rangle = \frac{1}{V_2}\int_{\Omega_0}Z_{Ab}^{\mathrm{T}}(\mathbf{x}')\left[-\int_{\Omega_2-\Omega_1}\hat{E}_{iJAb}G_{MJ,in}(\mathbf{x}-\mathbf{x}')\mathrm{d}V(\mathbf{x})\right]\mathrm{d}V(\mathbf{x}'). \tag{11}$$

Since Ω_1 and Ω_2 are ellipsoidal, it follows from the definition of Eshelby tensor, Eq. (8), that

$$\langle Z_{Mn}(\mathbf{x})\rangle = \frac{V_0}{V_2}(S_{MnAb}^2 - S_{MnAb}^1)\langle Z_{Ab}^{\mathrm{T}}(\mathbf{x}')\rangle, \tag{12}$$

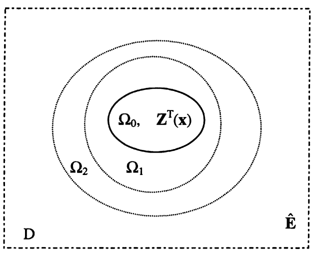

Fig. 1. An inclusion Ω_0 embedded in an infinite matrix, surrounded by two ellipsoidal surfaces Ω_1 and Ω_2.

where V_0 is the volume of inclusion Ω_0, and superscript r is used to denote properties belonging to phase r. In deriving Eq. (12), we have used the properties of the infinite-body Green's function, $G_{MJ}(\mathbf{x}-\mathbf{x}') = G_{MJ}(\mathbf{x}'-\mathbf{x})$, and $G_{MJ,in}(\mathbf{x}-\mathbf{x}') = G_{MJ,i'n'}(\mathbf{x}'-\mathbf{x})$. Eq. (12) is the generalization of Tanaka–Mori theorem in elasticity [2]. It shows that the average magnetoelectroelastic field in an annulus is completely determined by the average eigenfield in Ω_0, $\langle Z^{\mathrm{T}}_{Ab}\rangle$, and the magnetoelectroelastic Eshelby's tensors S^1_{MnAb} and S^2_{MnAb}, which correspond to the ellipsoidal domains Ω_1 and Ω_2. It does not depend on the shape and eigenfield distribution of the inclusion Ω_0. The average field vanishes in two situations, (1) Ω_1 and Ω_2 are similar and coaxial so that $S^1_{MnAb} = S^2_{MnAb}$; or (2) the average eigenfield in Ω_0, $\langle Z^{\mathrm{T}}_{Ab}\rangle$, vanishes.

3.3. Multi-inclusion problem

The generalized Tanaka–Mori theorem can be used to analyze the average field in a multi-inclusion embedded in an infinite matrix [17]. To this end let us consider an ellipsoidal inclusion Ω_2 containing another ellipsoidal inclusion Ω_1 imbedded in an infinite matrix D with magnetoelectroelastic moduli $\hat{E}_{iJAb}$; see Fig. 2. Ω_1 and Ω_2 do not need to be similar and coaxial. For convenience we also denote Ω_1 and and the annulus between Ω_2 and Ω_1 by Γ_1 and Γ_2, and its volume fraction by f_1 and f_2, with $f_1 + f_2 = 1$. The eigenfield in the double-inclusion is specified as

$$Z^{\mathrm{T}}_{Ab}(\mathbf{x}) = \sum_{r=1}^{2} \Theta_r(\mathbf{x}) Z^{\mathrm{T}}_{Ab}|_r, \tag{13}$$

where

$$\Theta_r(\mathbf{x}) = \begin{cases} 1, & \mathbf{x} \in \Gamma_r, \\ 0, & \mathbf{x} \notin \Gamma_r, \end{cases}$$

is the characterization function describing the topology of the double-inclusion. The eigenfield in both phases, $Z^{\mathrm{T}}_{Ab}|_1$ and $Z^{\mathrm{T}}_{Ab}|_2$, are assumed to be uniform, with $|_r$ used to denote quantities of phase r. Without external loading Z^0_{Ab} applied at boundary, the average field in the double-inclusion can be imagined to be due to two contributions, one is $Z^{\mathrm{T}}_{Ab}|_2$ in Ω_2, and the other is $[Z^{\mathrm{T}}_{Ab}|_1 - Z^{\mathrm{T}}_{Ab}|_2]$ in Ω_1. According to the linearity and Eqs. (7a) and (7b), the average field in Γ_1 is exactly given by

$$\langle Z_{Ab}\rangle_1 = S^2_{AbMn} Z^{\mathrm{T}}_{Mn}|_2 + S^1_{AbMn}(Z^{\mathrm{T}}_{Mn}|_1 - Z^{\mathrm{T}}_{Mn}|_2) = S^1_{AbMn} Z^{\mathrm{T}}_{Mn}|_1 + (S^2_{AbMn} - S^1_{AbMn}) Z^{\mathrm{T}}_{Mn}|_2, \tag{14a}$$

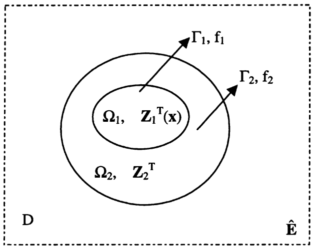

Fig. 2. A double-inclusion Ω_1 and Ω_2 embedded in an infinite matrix.

and

$$\langle \Sigma_{iJ} \rangle_1 = \hat{E}_{iJAb}(S^1_{AbMn} - I_{AbMn}) Z^{\mathrm{T}}_{Mn}|_1 + \hat{E}_{iJAb}(S^2_{AbMn} - S^1_{AbMn}) Z^{\mathrm{T}}_{Mn}|_2, \tag{14b}$$

where $\langle \cdot \rangle_r$ is used to denote volume average over Γ_r. In a similar manner the average fields in Γ_2 is given exactly by

$$\langle Z_{Ab} \rangle_2 = S^2_{AbMn} Z^{\mathrm{T}}_{Mn}|_2 + \frac{f_1}{f_2}(S^2_{AbMn} - S^1_{AbMn})(Z^{\mathrm{T}}_{Mn}|_1 - Z^{\mathrm{T}}_{Mn}|_2), \tag{15a}$$

and

$$\langle \Sigma_{iJ} \rangle_2 = \hat{E}_{iJAb}(S^2_{AbMn} - I_{AbMn}) Z^{\mathrm{T}}_{Mn}|_2 + \frac{f_1}{f_2} \hat{E}_{iJAb}(S^2_{AbMn} - S^1_{AbMn})(Z^{\mathrm{T}}_{Mn}|_1 - Z^{\mathrm{T}}_{Mn}|_2). \tag{15b}$$

The generalized Tanaka–Mori theorem, Eq. (12), has been used in deriving Eq. (15a). The average field in the double-inclusion can then be determined exactly from Eqs. (14a)–(15b) as

$$\langle Z_{Ab} \rangle = f_1 \langle Z_{Ab} \rangle_1 + f_2 \langle Z_{Ab} \rangle_2 = S^2_{AbMn}(f_1 Z^{\mathrm{T}}_{Mn}|_1 + f_2 Z^{\mathrm{T}}_{Mn}|_2) = S^2_{AbMn} \langle Z^{\mathrm{T}}_{Mn} \rangle \tag{16a}$$

and

$$\begin{aligned} \langle \Sigma_{iJ} \rangle &= f_1 \langle \Sigma_{iJ} \rangle_1 + f_2 \langle \Sigma_{iJ} \rangle_2 = \hat{E}_{iJAb}(S^2_{AbMn} - I_{AbMn})(f_1 Z^{\mathrm{T}}_{Mn}|_1 + f_2 Z^{\mathrm{T}}_{Mn}|_2) \\ &= \hat{E}_{iJAb}(S^2_{AbMn} - I_{AbMn}) \langle Z^{\mathrm{T}}_{Mn} \rangle, \end{aligned} \tag{16b}$$

where $\langle Z^{\mathrm{T}}_{Mn} \rangle$ is the average eigenfield in the double-inclusion. Eqs. (16a) and (16b) show that the average field in the double-inclusion is completely determined by the shape and orientation of Ω_2 and the average eigenfield in the double-inclusion, regardless of the shape and orientation of Ω_1.

The analysis for the double-inclusion can be easily extended to a multi-inclusion, in which the eigenfield is specified as

$$Z^{\mathrm{T}}_{Ab}(\mathbf{x}) = \sum_{r=1}^{n} \Theta_r(\mathbf{x}) Z^{\mathrm{T}}_{Ab}|_r. \tag{17}$$

Again, eigenfields in all the phases are assumed to be uniform. The average field in the multi-inclusion can be imagined to be due to the sum of eigenfield $[Z^{\mathrm{T}}_{Ab}|_r - Z^{\mathrm{T}}_{Ab}|_{r+1}]$ in $\Omega_r (r = 1 \to n-1)$, and $Z^{\mathrm{T}}_{Ab}|_n$ in Ω_n. The average field in Γ_α (with volume fraction f_α) due to the presence of eigenfield in Ω_β, $\langle Z_{Ab} \rangle_{\alpha\beta}$, is exactly given by

$$\langle Z_{Ab} \rangle_{\alpha\beta} = \begin{cases} \sum_{r=1}^{\beta} f_r / f_\alpha (S^\alpha_{AbMn} - S^{\alpha-1}_{AbMn})(Z^{\mathrm{T}}_{Mn}|_\beta - Z^{\mathrm{T}}_{Mn}|_{\beta+1}), & \Omega_\alpha \supset \Omega_\beta, \\ S^\beta_{AbMn}(Z^{\mathrm{T}}_{Mn}|_\beta - Z^{\mathrm{T}}_{Mn}|_{\beta+1}), & \Omega_\alpha \subseteq \Omega_\beta \neq \Omega_n, \\ S^n_{AbMn} Z^{\mathrm{T}}_{Mn}|_n, & \Omega_\beta = \Omega_n, \end{cases} \tag{18}$$

from which the average field over Γ_r is determined to be

$$\langle Z_{Ab}\rangle_1 = \sum_{r=1}^{n}\langle Z_{Ab}\rangle_{1r} = S^1_{AbMn}Z^{\mathrm{T}}_{Mn}|_1 + \sum_{r=2}^{n}(S^r_{AbMn} - S^{r-1}_{AbMn})Z^{\mathrm{T}}_{Mn}|_r \tag{19a}$$

and

$$\langle Z_{Ab}\rangle_r = \sum_{r'=1}^{n}\langle Z_{Ab}\rangle_{rr'} = \frac{S^r_{AbMn} - S^{r-1}_{AbMn}}{f_r}\sum_{r'=1}^{r-1} f_{r'}Z^{\mathrm{T}}_{Mn}|_{r'} + \left(S^r_{AbMn} - \frac{S^r_{AbMn} - S^{r-1}_{AbMn}}{f_r}\sum_{r'=1}^{r-1} f_{r'}\right)Z^{\mathrm{T}}_{Mn}|_r + \sum_{r'=r+1}^{n}(S^{r'}_{AbMn} - S^{r'-1}_{AbMn})Z^{\mathrm{T}}_{Mn}|_{r'}, \quad r = 2 \to n. \tag{19b}$$

When all Ω_r are of similar shape and coaxial, Eqs. (19a) and (19b) can be simplified as

$$\langle Z_{Ab}\rangle_r = S_{AbMn}Z^{\mathrm{T}}_{Mn}|_r, \quad r = 1 \to n \tag{20a}$$

and

$$\langle \Sigma_{iJ}\rangle_r = \hat{E}_{iJAb}(S_{AbMn} - I_{AbMn})Z^{\mathrm{T}}_{Mn}|_r, \quad r = 1 \to n, \tag{20b}$$

so that the average field in the multi-inclusion is still given by Eqs. (16a) and (16b), with S^2_{AbMn} replaced by S_{AbMn}.

3.4. Multi-inhomogeneity problem

The solution of multi-inclusion problem can be used to solve the multi-inhomogeneity problem, generalizing Eshelby's equivalent-inclusion concept [3]. We first consider an ellipsoidal inhomogeneity Ω_2 containing another ellipsoidal inhomogeneity Ω_1 imbedded in an infinite matrix D with magnetoelectroelastic moduli E_{iJAb}, see Fig. 3a. Ω_1 and Ω_2 do not need to be similar and coaxial. The magnetoelectroelastic moduli of the double-inhomogeneity can be specified as

$$\hat{E}_{iJAb}(\mathbf{x}) = \sum_{r=1}^{2}\Theta_r(\mathbf{x})\hat{E}^r_{iJAb}. \tag{21}$$

When a uniform field Z^{∞}_{Ab} is applied at the boundary, a disturbance field Z^{d}_{Ab} will be generated due to the presence of the inhomogeneities. The field in Ω_2, unlike that in a single inhomogeneity, is not uniform due to the presence of Ω_1. In such a case, we can define an equivalent double-inclusion with eigenfield $Z^{\mathrm{T}}_{Ab}|_1$ and $Z^{\mathrm{T}}_{Ab}|_2$, having exactly the same geometry as the double-inhomogeneity, as shown Fig. 3b, to represent the double-inhomogeneity. In order to insure the equivalency between the inclusion and inhomogeneity, the following consistency relationship should be satisfied for Γ_1 and Γ_2

$$\hat{E}^{\prime}_{iJAb}[Z^{\infty}_{Ab} + Z^{\mathrm{d}}_{Ab}] = \hat{E}_{iJAb}[Z^{\infty}_{Ab} + Z^{\mathrm{d}}_{Ab} - Z^{\mathrm{T}}_{Ab}], \tag{22a}$$

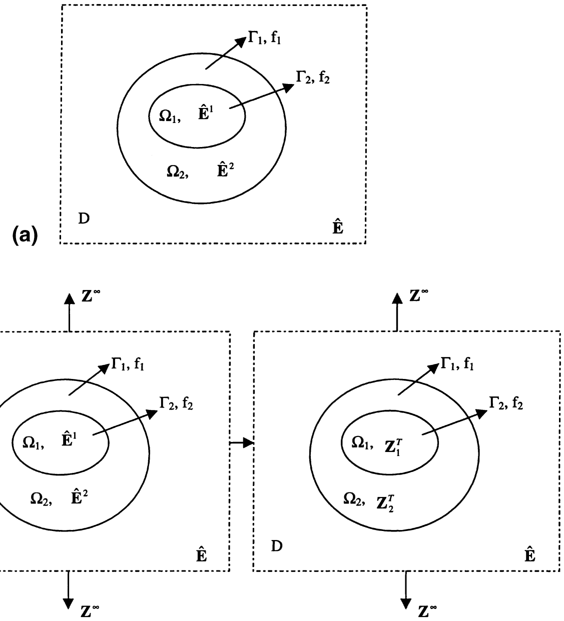

Fig. 3. A double-inhomogeneity Ω_1 and Ω_2 embedded in an infinite matrix: (a) the double inhomogeneity; (b) the equivalent double-inclusion.

where $\hat{E}^r_{iJAb}$ is the magnetoelectroelastic moduli of inhomogeneity, and Z^{T}_{Ab} is the eigenfield in the equivalent inclusion. Inserting Eqs. (14a) and (15a) into Eq. (22a) yields

$$\begin{aligned}&\hat{E}^1_{iJAb}[Z^\infty_{Ab} + S^1_{AbMn}Z^{\mathrm{T}}_{Mn}|_1 + (S^2_{AbMn} - S^1_{AbMn})Z^{\mathrm{T}}_{Mn}|_2]\\ &\quad = \hat{E}_{iJAb}[Z^\infty_{Ab} + (S^2_{AbMn} - I_{AbMn})Z^{\mathrm{T}}_{Mn}|_1 + (S^2_{AbMn} - S^1_{AbMn})Z^{\mathrm{T}}_{Mn}|_2] \qquad (22b)\end{aligned}$$

and

$$\begin{aligned}&\hat{E}^2_{iJAb}[Z^\infty_{Ab} + S^2_{AbMn}Z^{\mathrm{T}}_{Mn}|_2 + \frac{f_1}{f_2}(S^2_{AbMn} - S^1_{AbMn})(Z^{\mathrm{T}}_{Mn}|_1 - Z^{\mathrm{T}}_{Mn}|_2)]\\ &\quad = \hat{E}_{iJAb}[Z^\infty_{Ab} + (S^2_{AbMn} - I_{AbMn})Z^{\mathrm{T}}_{Mn}|_2 + \frac{f_1}{f_2}(S^2_{AbMn} - S^1_{AbMn})(Z^{\mathrm{T}}_{Mn}|_1 - Z^{\mathrm{T}}_{Mn}|_2)], \qquad (22c)\end{aligned}$$

where b and c are consistency relationships for Γ_1 and Γ_2, respectively. The left-hand side of the equation denotes actual field in the double-inhomogeneity, while the right-hand side of equation represents the field in the equivalent double-inclusion. Eqs. (22a)–(22c) can be solved to yield the eigenfield in the double-inclusion, $Z^{\mathrm{T}}_{Ab}|_r$, as function of far-field loading Z^∞_{Ab}, and the average disturbance field in the double-inhomogeneity can then be determined from Eqs. (16a) and (16b). When Ω_1 and Ω_2 are similar and coaxial, we will have

$$Z^{\mathrm{T}}_{Ab}|_r = [(\hat{E}_{iJAb} - \hat{E}^r_{iJAb})^{-1}\hat{E}_{iJMn} - S_{AbMn}]^{-1}Z^{\infty}_{Mn}, \quad r = 1, 2. \tag{23}$$

The generalization to the multi-inhomogeneity is straightforward. For coaxial multi-inhomogeneity with similar shape, Eqs. (23), (20a) and (20b) are still valid, with r range from 1 to n.

3.5. Multi-inhomogeneous-inclusion problem

We further consider the multi-inhomogeneous-inclusion problem, where the inhomogeneity not only has different magnetoelectroelastic moduli from the matrix, but also has different eigenfield due to, for example, different thermal moduli. We first consider the double-inhomogeneous-inclusion as shown in Fig. 4a, where an ellipsoidal inhomogeneous-inclusion Ω_2 containing another ellipsoidal inhomogeneous-inclusion Ω_1 is imbedded in an infinite matrix D with magnetoelectroelastic moduli $\hat{E}_{iJAb}$. The magnetoelectroelastic moduli and thermal moduli of the double-inhomogeneous-inclusion can be specified as

$$\hat{E}_{iJAb}(\mathbf{x}) = \sum_{r=1}^{2}\Theta_r(\mathbf{x})\hat{E}^r_{iJAb} \tag{24a}$$

and

$$Z^{\mathrm{T}}_{Ab}(\mathbf{x}) = \sum_{r=1}^{2}\Theta_r(\mathbf{x})Z^{\mathrm{T}}_{Ab}|_r. \tag{24b}$$

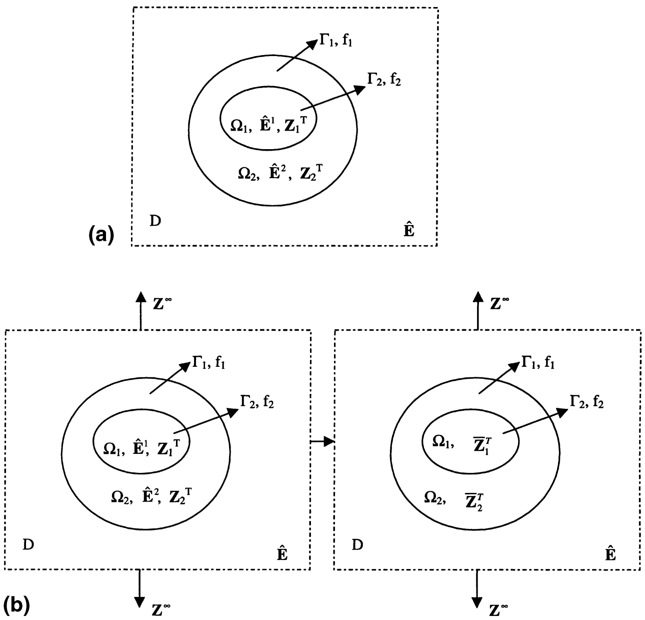

Fig. 4. A double-inhomogeneous-inclusion Ω_1 and Ω_2 embedded in an infinite matrix: (a) the double-inhomogeneous-inclusion; (b) the equivalent double-inclusion.

When a uniform field Z^{∞}_{Ab} is applied at the boundary of infinite matrix, a disturbance field Z^{d}_{Ab} will be generated due to the presence of the inhomogeneous-inclusion. As in the case of double-inhomogeneity, we can define an equivalent double-inclusion with eigenfield $Z^{*}_{Ab}|_1$ and $Z^{*}_{Ab}|_2$, having exact same geometry as the double-inhomogeneous-inclusion, as shown in Fig. 4b, to represent the double-inhomogeneous-inclusion. In order to insure the equivalence, the following consistency relationship should be satisfied by Γ_1 and Γ_2

$$\hat{E}'_{iJAb}[Z^{\infty}_{Ab} + Z^{\mathrm{d}}_{Ab} - Z^{\mathrm{T}}_{Ab}|_r] = \hat{E}_{iJAb}[Z^{\infty}_{Ab} + Z^{\mathrm{d}}_{Ab} - Z^{\mathrm{T}}_{Ab}|_r - Z^{*}_{Ab}|_r] = E_{iJAb}[Z^{\infty}_{Ab} + Z^{\mathrm{d}}_{Ab} - \bar{Z}^{\mathrm{T}}_{Ab}|_r], \tag{25a}$$

where $\bar{Z}^{\mathrm{T}}_{Ab}|_r = Z^{\mathrm{T}}_{Ab}|_r + Z^{*}_{Ab}|_r$ is the equivalent eigenfield in the double-inclusion. Inserting Eqs. (14a) and (15a) into Eq. (25a) yields

$$\begin{aligned}\hat{E}^1_{iJAb}[Z^{\infty}_{Ab} &+ S^1_{AbMn}\bar{Z}^{\mathrm{T}}_{Mn}|_1 + (S^2_{AbMn} - S^1_{AbMn})\bar{Z}^{\mathrm{T}}_{Mn}|_2 - Z^{\mathrm{T}}_{Ab}|_1] \\ &= \hat{E}_{iJAb}[Z^{\infty}_{Ab} + (S^1_{AbMn} - I_{AbMn})\bar{Z}^{\mathrm{T}}_{Mn}|_1 + (S^2_{AbMn} - S^1_{AbMn})\bar{Z}^{\mathrm{T}}_{Mn}|_2]\end{aligned} \tag{25b}$$

and

$$\begin{aligned}\hat{E}^2_{iJAb}[Z^{\infty}_{Ab} &+ S^2_{AbMn}\bar{Z}^{\mathrm{T}}_{Mn}|_2 + \frac{f_1}{f_2}(S^2_{AbMn} - S^1_{AbMn})(\bar{Z}^{\mathrm{T}}_{Mn}|_1 - \bar{Z}^{\mathrm{T}}_{Mn}|_2) - Z^{\mathrm{T}}_{Ab}|_2] \\ &= \hat{E}_{iJAb}[Z^{\infty}_{Ab} + (S^2_{AbMn} - I_{AbMn})\bar{Z}^{\mathrm{T}}_{Mn}|_2 + \frac{f_1}{f_2}(S^2_{AbMn} - S^1_{AbMn})(\bar{Z}^{\mathrm{T}}_{Mn}|_1 - \bar{Z}^{\mathrm{T}}_{Mn}|_2)].\end{aligned} \tag{25c}$$

Eqs. (25a)–(25c) can be solved to yield the eigenfield in the double-inclusion, $\bar{Z}^{\mathrm{T}}_{Ab}|_r$, and the average disturbance field in the double-inhomogeneous-inclusion can then be determined from Eqs. (16a) and (16b). When Ω_1 and Ω_2 are similar and coaxial, we will have

$$\begin{aligned}Z^{*}_{Ab}|_r = {}&[(\hat{E}_{iJAb} - \hat{E}^r_{iJAb})^{-1}\hat{E}_{iJMn} - S_{AbMn}]^{-1}Z^{\infty}_{Mn} \\ &+ [(\hat{E}_{iJAb} - \hat{E}^r_{iJAb})^{-1}\hat{E}_{iJMn} - S_{AbMn}]^{-1}(S_{MnKl} - I_{MnKl})Z^{\mathrm{T}}_{Kl}|_r \quad r = 1, 2.\end{aligned} \tag{26}$$

The generalization to the multi-inhomogeneity is straightforward. For coaxial multi-inhomogeneity with similar shape, Eqs. (20a), (20b) and (26) are still valid, with r range from 1 to n.

4. Double- and multi-inclusion model

The results presented in Section 3 can serve as a basis for an averaging scheme to predict the effective magnetoelectroelastic moduli of heterogeneous materials. The scheme generalizes the multi-inclusion model of Hori and Nemat-Nasser on the effective elastic moduli [4], and that of Li on the effective thermal expansion coefficient [5]. We will discuss these two aspects in the following subsections.

4.1. The effective magnetoelectroelastic moduli

The effective magnetoelectroelastic moduli of a composite composed of matrix phase 2 with magnetoelectroelastic moduli $\hat{E}^2_{iJAb}$, and reinforcement 1 with moduli $\hat{E}^1_{iJAb}$, subjected to external loading Z^0_{Ab} at the boundary, can be approximated by the effective moduli of the double-inhomogeneity shown in Fig. 3. No temperature change is assumed to exist so that the eigenfield is zero in both phases. Note that at the boundary of the infinite body shown in Fig. 3b, it is Z^{∞}_{Ab}, not Z^0_{Ab}, that is assume to be applied. Z^{∞}_{Ab} is chosen in such a way that it yields an average field Z^0_{Ab} in the double inhomogeneity, and thus also in the considered composite. From the definition of the effective moduli, we have $\Sigma^{\infty}_{iJ} + \langle \Sigma^{\mathrm{d}}_{iJ} \rangle = \hat{E}^*_{iJAb}(Z^{\infty}_{Ab} + \langle Z^{\mathrm{d}}_{Ab} \rangle)$, where the average disturbance field $\langle Z^{\mathrm{d}}_{Ab} \rangle$ in the double-inhomogeneity can be obtained from Eqs. (16a) and (16b) as function of $\langle Z^{\mathrm{T}}_{Ab} \rangle$, so that the effective moduli of the double-inhomogeneity (thus the composite materials) is given by

$$\hat{E}^*_{iJAb} = \hat{E}_{iJMn}[I_{MnKl} + (S^2_{MnCd} - I_{MnCd})A_{CdKl}][I_{KlAb} + S^2_{KlEf}A_{EfAb}]^{-1} \tag{27}$$

with A_{AbMn} defined by

$$A_{AbMn}Z^{\infty}_{Mn} = \sum_{r=1}^{2} f_r Z^{\mathrm{T}}_{Ab}|_r. \tag{28}$$

The equivalent eigenfield $Z^{\mathrm{T}}_{Ab}|_r$ can be determined from the consistency equations (22a) and (22b). In case of composites with aligned reinforcement of identical shape, $Z^{\mathrm{T}}_{Ab}|_r$ is given by Eq. (23). The extension to the multi-phase composite is straightforward. When the reinforcements are aligned and of similar shape, the equivalent eigenfield is given by Eq. (23) ranging from 1 to n, and the effective moduli are given by

$$\hat{E}^*_{iJAb} = \hat{E}_{iJMn}[I_{MnKl} + (S_{MnCd} - I_{MnCd})R_{CdKl}][I_{MnKl} + S_{MnCd}R_{CdKl}]^{-1} \tag{29}$$

with $R_{AbMn} = \sum_{r=1}^{n} f_r R^r_{AbMn}$, and $R^r_{AbMn} = [(\hat{E}_{iJAb} - \hat{E}^r_{iJAb})^{-1}\hat{E}_{iJMn} - S_{AbMn}]^{-1}$.

4.2. The effective thermal moduli

The effective thermal moduli of a composite composed of matrix phase 2 with magnetoelectroelastic moduli $\hat{E}^2_{iJAb}$ and thermal moduli $\Pi_{Kl}|_2$, and reinforcement 1 with magnetoelectroelastic moduli E^1_{iJAb} and thermal moduli $\Pi_{Kl}|_1$, subjected to zero Z^0_{Kl} at the boundary, can be approximated by the effective moduli of the double-inhomogeneous-inclusion in Fig. 4. The eigenfield in the inhomogeneous-inclusion is $Z^{\mathrm{T}}_{Kl}|_r = (\hat{E}^r)^{-1}_{KliJ}\Pi_{iJ}|_r\theta$. In this situation, the applied field at the boundary of the infinite medium should be chosen such that the average field in the composite is zero. When the reinforcement is aligned and of identical shape, it is determined from Eq. (26)

$$Z^{\infty}_{Ji} = -(I_{JiMn} + S_{JiAb}R_{AbMn})^{-1}\sum_{r=1}^{2} f_r S_{MnEf}[R^r_{EfGh}(S_{GhCd} - I_{GhCd}) + I_{EfCd}]^{-1}Z^{\mathrm{T}}_{cD}|_r. \tag{30}$$

The average field in the double-inhomogeneity can then be obtained from Eqs. (16a), (16b) and (26), and the effective thermal moduli of the double-inhomogeneity (thus the composite materials), according to $\Pi^*_{iJ}\theta = -\langle \Sigma_{iJ} \rangle$, is given by

$$\Pi^*_{iJ} = \hat{E}_{iJKl}(I_{KlAb} + R_{KlCd}S_{CdAb})^{-1}\sum_{r=1}^{2} f_r[R^r_{AbEf}(S_{EfGh} - I_{EfGh}) + I_{AbGh}](\hat{E}^r)^{-1}_{GhlM}\Pi^r_{lM}. \tag{31}$$

The extension to the multi-phase composite is straightforward. When all the reinforcements are aligned and of similar shape, Eq. (31) is still valid, with the summation raging from 1 to n.

From Eqs. (27) and (31), it is clear that the estimated effective moduli not only depend on the magnetoelectroelastic moduli of constituents, but also depend on the magnetoelectroelastic moduli of infinite matrix, $\hat{E}_{iJAb}$, which can be chosen arbitrarily. When the magnetoelectroelastic moduli of the matrix are assigned to the infinite medium, the generalized Mori–Tanaka approach is recovered [15,18,32]. If the unknown effective moduli of the composite are assigned instead, the self-consistent approach is recovered. This is also true for elastic composites, as shown by Nemat-Nasser and Hori [4]. They further showed that the effective moduli predicted by the double-inclusion model comply with variational bounds. Such an evaluation cannot be made here, since the variational bounds for magnetoelectroelastic moduli is yet to be developed.

5. Numerical results and discussion

In this section, we will present some numerical results to demonstrate the applicability of the theory. We will consider a transversely isotropic material exhibiting full coupling between static elastic, electric, and magnetic fields, with unique axis along x_3 direction. The independent material constants are the elastic constants C_{11}, C_{12}, C_{13}, C_{33}, and C_{44}; piezoelectric constants e_{31}, e_{33}, and e_{15}; piezomagnetic constants q_{31}, q_{33}, and q_{15}; dielectric constants κ_{11} and κ_{33}; magnetoelectric constants a_{11} and a_{33}; magnetic constants μ_{11} and μ_{33}; thermal stress constants λ_{11} and λ_{33}; pyroelectric constant p_3; and pyromagnetic constant m_3. This is the most general situation, and for a particular material, some of the coupling coefficients may be zero.

5.1. Magnetoelectroelastic Eshelby tensors

We first demonstrate the applicability of the numerical algorithm for evaluation the magnetoelectroelastic Eshelby's tensors, which is implemented in a FORTRAN program. We have calculated the magnetoelectroelastic Eshelby's tensors numerically for circular cylindrical inclusion and thin-disc inclusions, and compared them with the available exact closed-form expression obtained by Li and Dunn [1]. The material moduli we used are listed in Table 3, while the comparisons are listed in Table 4. We choose U and V to be 16 and 64, respectively, and the aspect ratios for cylindrical and thin-disc inclusion to be 10^6 and 10^{-6}, respectively. It is found that the numerical results agree with exact solutions at fifth significant digit. Thus the developed algorithm can be used to evaluate magnetoelectroelastic Eshelby's tensors accurately.

Table 3
Material constant for Eshelby's tensors calculation[a]

C_{11}	C_{12}	C_{13}	C_{33}	C_{44}	a_{11}
286	173	170	269.5	45.3	0.005×10^{-9}
e_{15}	e_{31}	e_{33}	κ_{11}	κ_{33}	a_{33}
11.6	−4.4	18.6	0.08×10^{-9}	0.093×10^{-9}	0.003×10^{-9}
q_{15}	q_{31}	q_{33}	μ_{11}	μ_{33}	μ_{33}
550	580.3	699.7	-590×10^{-6}	157×10^{-6}	157×10^{-6}

[a] Units: elastic constants, GPa; dielectric constants, C^2/Nm^2; magnetic constants, N s^2/C^2; piezoelectric constants, C/m^2; piezomagnetic constants, N/Am; magnetoelectric coefficients, Ns/VC.

Table 4
Comparisons between Eshelby's tensors evaluated by numerical integration and exact solution

Cylindrical	S_{1111}	S_{1122}	S_{1133}	$2S_{2323}$, S_{4141}, S_{5151}	S_{1212}	S_{1143} $(\times 10^{-11})$	S_{1153} $(\times 10^{-8})$
Numerical	0.70061	0.10184	0.29808	0.5	0.59878	−0.76923	0.10145
Exact	0.70061	0.10184	0.29808	0.5	0.59878	−0.76923	0.10145
Thin-disc	S_{3311}	$2S_{2323}$, S_{3333}, S_{4343}, S_{5353}	S_{2342} $(\times 10^{-9})$	S_{2352} $(\times 10^{-7})$	S_{4311} $(\times 10^{11})$	S_{5311} $(\times 10^{-7})$	
Numerical	−0.17706	1	0.25607	0.12141	0.11910	−0.44855	
Exact	−0.17706	1	0.25607	0.12141	0.11910	−0.44855	

5.2. The effective magnetoelectroelastic moduli

We then applied the multi-inclusion model to predict the effective magnetoelectroelastic moduli of a piezoelectric–piezomagnetic composite. Piezoelectric phase is $BaTiO_3$, while piezomagnetic phase is $CeFe_2O_4$. The magnetoelectroelastic moduli of both phases are listed in Table 5. Assigning the material properties of piezomagnetic phase $CeFe_2O_4$ to the infinite medium, we are able to estimate the effective magnetoelectroelastic moduli of $BaTiO_3$ fiber reinforced $CeFe_2O_4$, and $BaTiO_3$–$CeFe_2O_4$ laminate. Neither phase shows magnetoelectric coupling. The composites, however, show magnetoelectric coupling, demonstrated by the non-zero magnetoelectric coefficients a^*_{11} and a^*_{11}, as shown in Fig. 5. It is observed that in fibrous composites, a^*_{33} is three orders larger than a^*_{11}, both being positive, while in laminated composites, a^*_{11} is three orders larger than a^*_{33}, both being negative. These dramatic differences in the composites of different microgeometry can be explained by the following argument. In fibrous composites, when E_3 is applied at the boundary of both phases, σ_{11} and σ_{33} are induced in the piezoelectric phase. As required by the continuity of traction, σ_{11} is also induced in the piezomagnetic phase. This second-order stress causes H_3 in piezoelectric phase, and then H_3 in the piezoelectric phase because H_3 is continuous across phase boundary. Since we know from the boundary condition that average H_3 is zero in composite, there must be B_3 in the piezomagnetic phase to cancel the H_3 caused by the second-order stress. However, when E_1 is applied at the

Table 5
Materials properties of $BaTiO_3$ and $CoFeO_4$[a]

	C_{11}	C_{12}	C_{13}	C_{33}	C_{44}
$BaTiO_3$	166	77	78	162	43
$CoFe_2O_4$	286	173	170	269.5	45.3
	e_{15}	e_{31}	e_{33}	κ_{11}	κ_{33}
$BaTiO_3$	11.6	−4.4	18.6	11.2×10^{-9}	12.6×10^{-9}
$CoFe_2O_4$	0	0	0	0.08×10^{-9}	0.093×10^{-9}
	q_{15}	q_{31}	q_{33}	μ_{11}	μ_{33}
$BaTiO_3$	0	0	0	5×10^{-6}	10×10^{-6}
$CoFe_2O_4$	550	580.3	699.7	-590×10^{-6}	157×10^{-6}

[a] Units: elastic constants, GPa; dielectric constants, C^2/Nm^2; magnetic constants, Ns^2/C^2; piezoelectric constants, C/m^2; piezomagnetic constants, N/Am; magnetoelectric coefficients, Ns/VC.

boundary of both phases of a fibrous composite, σ_{13} is induced in the piezoelectric phase first, and then in the piezomagnetic phase owing to the traction continuity at the phase boundary. This σ_{13} induces H_1 in the piezomagnetic phase. Then H_1 is induced in the piezoelectric phase to maintain an overall zero magnetic field in the composite; this H_1 induces B_1 in the piezoelectric phase. The difference between a^*_{11} and a^*_{33} is due to the difference in the magnetic constants of the piezoelectric and piezomagnetic phases. For a^*_{33}, B_3 is caused by the piezomagnetic phase; for a^*_{11}, B_1 is caused by the piezoelectric phase, as we just discussed. Since the magnetic constant of the piezomagnetic phase is two orders larger than that of piezoelectric phase, a^*_{33} is three orders larger than a^*_{11} in fibrous composite. Similar reasoning explains why a^*_{11} is three orders larger than a^*_{33} in laminated composite, as well as the sign difference of magnetoelectric coefficients in fibrous and laminated composites.

Finally, it is worthwhile to note that there is an order of magnitude difference between the predicted and measured magnetoelectric coefficients for the practical composites. The reason is probably due to the extent of poling for the piezoelectric and piezomagnetic constituents. That is, the grain orientation distributions in piezoelectric and piezomagnetic phases may not be in optimized distribution, and thus, the piezoelectric constants and piezomagnetic constants in constituents may have not achieved the values used in the calculations. The porosity and microcracks also tends to degrade the performance of the constituents and composites. To overcome this difficulty, it is necessary to realize the maximum piezoelectric effect in piezoelectric phase, maximum piezomagnetic effect in piezomagnetic phase, and maximum interaction between the piezoelectric and piezomagnetic phases. The maximum piezoelectric and piezomagnetic phases can be achieved by carefully tailoring the texture in the constituent materials, for example, by the epitaxial film growth; the effects of texture on the overall piezoelectric moduli have been discussed in [33,34]. To maximize the interaction between the piezoelectric and piezomagnetic phases, a diversion from the fibrous or laminated configuration may be necessary, as well as additional phases. For example, the addition of a conducting phase in the piezomagnetic material will

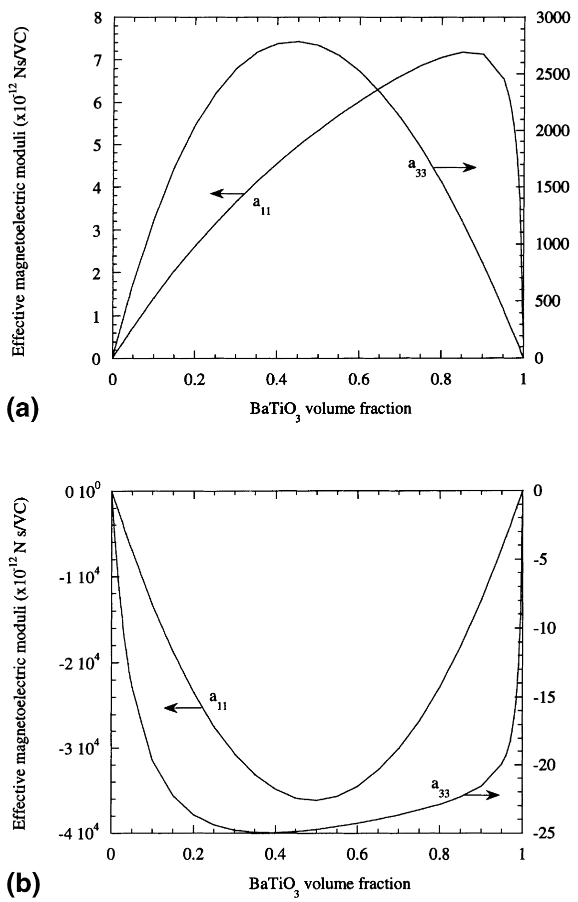

Fig. 5. Magnetoelectric coefficients of piezoelectric-piezomagnetic composites: (a) fibrous composite; (b) laminated composite.

increase its dielectric constant, and thus, effectively increase the local electric field in piezoelectric phase, and enhance its piezoelectric response.

6. Conclusions

The multi-inclusion and inhomogeneity problems in a magnetoelectroelastic solid have been studied. A numerical algorithm is developed to evaluate magnetoelectroelastic Eshelby's tensors. It is shown that the average field in an annulus (between two ellipsoidal surfaces) surrounding an inclusion embedded in an infinite matrix will only depend on the shapes and orientations of the two ellipsoids, from which the exact average field in a multi-inclusion embedded in an infinite matrix is obtained. The average field in a multi-inhomogeneity is then solved using the concept of equivalent multi-inclusion. The solutions of multi-inclusion and inhomogeneity problems serve as basis for an averaging scheme to model the effective magnetoelectroelastic moduli of heterogeneous materials. Some numerical results have been presented to demonstrate the applicability of the algorithm, and the proposed multi-inclusion model. The potential techniques to enhance the magnetoelectric effect in the practical composite are also discussed.

References

[1] J.Y. Li, M.L. Dunn, Philos. Mag. A 77 (1998) 1341.
[2] K. Tanaka, T. Mori, J. Elasticity 2 (1972) 199.
[3] J.D. Eshelby, Proc. R. Soc. Lond. A 241 (1957) 376.
[4] M. Hori, S. Nemat-Nasser, J. Eng. Mater. Technol. 116 (1994) 305.
[5] J.Y. Li, Int. J. Solids Struct., in press.
[6] A.M.J.G. VanRun, D.R. Terrell, J.H. Scholing, J. Mater. Sci. 9 (1974) 1710.
[7] L.P.M. Bracke, R.G. Van Vliet, Int. J. Electron. 51 (1981) 255.
[8] G. Harshe, J.P. Dougherty, R.E. Newnham, Int. J. Appl. Electromagn. Mater. 4 (1993) 145.
[9] G. Harshe, J.P. Dougherty, R.E. Newnham, Int. J. Appl. Electromagn. Mater. 4 (1993) 161.
[10] M. Avellaneda, G. Harshe, J. Intelligent Mater. Syst. Struct. 5 (1994) 501.
[11] C.W. Nan, Phys. Rev. B 50 (1994) 6082.
[12] J.H. Huang, W.S. Kuo, J. Appl. Phys. 81 (1997) 1378.
[13] Y. Benveniste, Phys. Rev. B 51 (1995) 424.
[14] Y. Benveniste, G.J. Dvorak, J. Mech. Phys. Solids 40 (1992) 1295.
[15] J.Y. Li, M.L. Dunn, J. Intelligent Mater. Syst. Struct. 9 (1999) 404.
[16] T. Mura, Micromechanics of Defects in Solids, second ed., Martinus Nijhoff, Dordrecht, The Netherlands, 1987.
[17] S. Nemat-Nasser, M. Hori, Micromechanics: Overall Properties of Heterogeneous Materials, Elsevier, Amsterdan, 1993.
[18] T. Mori, K. Tanaka, Acta Metall. 21 (1973) 571.
[19] W.F. Deeg, The analysis of dislocation, crack, and inclusion problems in piezoelectric solids, Ph.D. Dissertation, Stanford University, Stanford, California, 1980.
[20] B. Wang, Int. J. Solids Struct. 29 (1992) 293.
[21] Y. Benveniste, J. Appl. Phys. 72 (1992) 1086.
[22] M.L. Dunn, M. Taya, Proc. R. Soc. Lond. A 443 (1993) 265.
[23] T. Chen, J. Mech. Phys. Solids 41 (1993) 1781.
[24] T. Chen, Mech. Res. Commun. 20 (1993) 271.
[25] M.L. Dunn, H.A. Wienecke, Int. J. Solids Struct. 33 (1996) 4571.
[26] M.L. Dunn, H.A. Wienecke, Int. J. Solids Struct. 34 (1997) 357.
[27] J.F. Nye, Physical Properties of Crystals, Oxford University Press, Oxford, 1957.
[28] D.M. Barnett, J. Lothe, Phys. Stat. Sol. (b) 67 (1975) 105.
[29] V.I. Alshits, A.N. Darinskii, J. Lothe, Wave Motion 16 (1992) 265.
[30] A.C. Gavazzi, D.C. Lagoudas, Comput. Mech. 7 (1990) 13.
[31] W.H. Press, S.A. Teukolsky, W.T. Vetterling, B.P. Flannery, Numerical Recipes in FORTRAN, second ed., Cambridge University Press, Cambridge, 1992.
[32] M.L. Dunn, M. Taya, Int. J. Solids Struct. 30 (1993) 161.
[33] J.Y. Li, M.L. Dunn, H. Ledbetter, J. Appl. Phys. 86 (1999) 4626.
[34] J.Y. Li, J. Mech. Phys. Solids 48 (2000) 529.